

# Northumbria Research Link

Citation: Hayes, Samuel, Lim, Michael, Whalen, Dustin, Mann, Paul, Fraser, Paul, Penlington, Roger and Martin, James (2022) The Role of Massive Ice and Exposed Headwall Properties on Retrogressive Thaw Slump Activity. *Journal of Geophysical Research: Earth Surface*, 127 (11). e2022JF006602. ISSN 2169-9003

Published by: American Geophysical Union

URL: <https://doi.org/10.1029/2022JF006602> <<https://doi.org/10.1029/2022JF006602>>

This version was downloaded from Northumbria Research Link:  
<https://nrl.northumbria.ac.uk/id/eprint/50714/>

Northumbria University has developed Northumbria Research Link (NRL) to enable users to access the University's research output. Copyright © and moral rights for items on NRL are retained by the individual author(s) and/or other copyright owners. Single copies of full items can be reproduced, displayed or performed, and given to third parties in any format or medium for personal research or study, educational, or not-for-profit purposes without prior permission or charge, provided the authors, title and full bibliographic details are given, as well as a hyperlink and/or URL to the original metadata page. The content must not be changed in any way. Full items must not be sold commercially in any format or medium without formal permission of the copyright holder. The full policy is available online: <http://nrl.northumbria.ac.uk/policies.html>

This document may differ from the final, published version of the research and has been made available online in accordance with publisher policies. To read and/or cite from the published version of the research, please visit the publisher's website (a subscription may be required.)

## The Role of Massive Ice and Exposed Headwall Properties on Retrogressive Thaw Slump Activity

Samuel Hayes<sup>1,2</sup> , Michael Lim<sup>3</sup> , Dustin Whalen<sup>4</sup> , Paul J. Mann<sup>3</sup> , Paul Fraser<sup>4</sup>, Roger Penlington<sup>3</sup> , and James Martin<sup>3</sup>

<sup>1</sup>School of Biological, Earth and Environmental Sciences, University College Cork, Cork, Ireland, <sup>2</sup>Department of Geography, University College Cork, Cork, Ireland, <sup>3</sup>Engineering and Environment, Northumbria University, Newcastle upon Tyne, UK, <sup>4</sup>Natural Resources Canada, Geological Survey of Canada—Atlantic, Dartmouth, NS, Canada

### Key Points:

- Active headwall properties strongly influence rates of headwall retreat
- Passive seismic monitoring is an effective tool for detecting and mapping massive ice surface variability
- Subsurface massive ice and overburden thickness display variations not predicted from extrapolations of headwall exposures

### Correspondence to:

S. Hayes,  
shayes@ucc.ie

### Citation:

Hayes, S., Lim, M., Whalen, D., Mann, P. J., Fraser, P., Penlington, R., & Martin, J. (2022). The role of massive ice and exposed headwall properties on retrogressive thaw slump activity. *Journal of Geophysical Research: Earth Surface*, 127, e2022JF006602. <https://doi.org/10.1029/2022JF006602>

Received 13 JAN 2022  
Accepted 14 NOV 2022

### Author Contributions:

**Conceptualization:** Samuel Hayes  
**Data curation:** Samuel Hayes  
**Formal analysis:** Samuel Hayes  
**Funding acquisition:** Samuel Hayes, Michael Lim, Dustin Whalen, Paul J. Mann, Paul Fraser  
**Investigation:** Samuel Hayes, Dustin Whalen, Paul Fraser  
**Methodology:** Samuel Hayes  
**Project Administration:** Samuel Hayes, Michael Lim, Dustin Whalen, Paul J. Mann, Paul Fraser  
**Resources:** Samuel Hayes, Michael Lim, Dustin Whalen, Paul Fraser  
**Supervision:** Michael Lim, Paul J. Mann, Roger Penlington, James Martin  
**Validation:** Samuel Hayes  
**Visualization:** Samuel Hayes  
**Writing – original draft:** Samuel Hayes  
**Writing – review & editing:** Samuel Hayes, Michael Lim, Paul J. Mann

© 2022 The Authors.

This is an open access article under the terms of the [Creative Commons Attribution-NonCommercial License](https://creativecommons.org/licenses/by-nc/4.0/), which permits use, distribution and reproduction in any medium, provided the original work is properly cited and is not used for commercial purposes.

**Abstract** Retrogressive Thaw Slumps (RTSs), a highly dynamic form of mass wasting, are accelerating geomorphic change across ice-cored permafrost terrain, yet the main controls on their activity are poorly constrained. Questions over the spatial variability of environmentally sensitive massive ice bodies and a paucity of high-spatial and temporal resolution topographic data have limited our ability to project their development and wider impacts. This research addresses these key problems by investigating RTS processes on Peninsula Point—a well-studied site for intra-sedimental massive ice in the Western Canadian Arctic. Utilizing high-resolution topographic data from drone surveys in 2016, 2017 and 2018 we (a) measure the temporal and spatial variations in headwall properties and retreat rates, (b) determine the spatial pattern of subsurface layering using passive seismic monitoring and (c) combine these to analyze and contextualize the factors controlling headwall retreat (HWR) rates. We find that headwall properties, namely massive ice and overburden thickness, are significant controls over rates of HWR. Where persistent massive ice exposures are present inland of the headwall, regardless of thickness, and overburden thickness remains <4 m, HWR is typically more than double that of other headwalls. Furthermore, a 3D site model was created by combining photogrammetric and passive seismic data, highlighting internal layering variability and demonstrating the limitations of extrapolations of internal layering based on headwall exposures. These results provide fresh insights into the in situ controls on HWR rates and new approaches to understanding their variability.

**Plain Language Summary** Retrogressive thaw slumps (thaw slumps) are a form of landslide that occurs when thick layers of ice under the ground are exposed and thaw, creating muddy flows that can grow to cover thousands of m<sup>2</sup> in just a few years. These processes are occurring more frequently in the western Canadian Arctic during the last two decades, becoming one of the primary causes of landscape change. This research examines how variation in the ice and overlying soil thickness of the thaw slump headwalls (a prominent, near vertical cliff at the back of a thaw slump), affects their rate of growth. We find that a persistent layer of ice, and a thin soil overburden, tends to promote headwall retreat rates much faster than otherwise. We also show how simple, cost-effective and quick measurements can be used to map the ice layers and show how they vary inland. This research suggests that detailed knowledge of how the internal ice and overburden layering varies is critical to understanding how thaw slumps evolve and to predict their development.

## 1. Introduction

Unlithified Arctic coastlines are situated on the boundary of three rapidly changing and intertwined systems—terrestrial, oceanic, and atmospheric. Near surface terrestrial permafrost temperatures are increasing (Biskaborn et al., 2019), and active layer depths (ALDs) are thickening (Letterly, 2018). Sea ice cover is in a state of rapid decline, and ocean temperatures are increasing (Markus et al., 2009; Steele et al., 2008; Stroeve et al., 2014). Surface air temperatures are warming at an accelerated rate relative to the rest of the planet (Johannessen et al., 2016; Serreze & Francis, 2006). All these changes are expected to continue through the 21st century in response to anthropogenic climate change (AMAP, 2017; Collins et al., 2013; Comiso, 2006). These profound transformations of the Arctic environment are already resulting in significant widespread degradation of coastal permafrost (Fritz et al., 2017; Günther et al., 2013, 2015; Jones et al., 2018; Lewkowicz & Way, 2019; Mars & Houseknecht, 2007; Novikova et al., 2018; Pizhankova, 2016; Ramage et al., 2018), with further degradation likely in the coming decades (Irrgang et al., 2022). One of the most active forms of thermokarst are Retrogressive Thaw Slumps (RTSs), a form of slope failure that occurs in ice rich permafrost in which thawed soils and ice melt

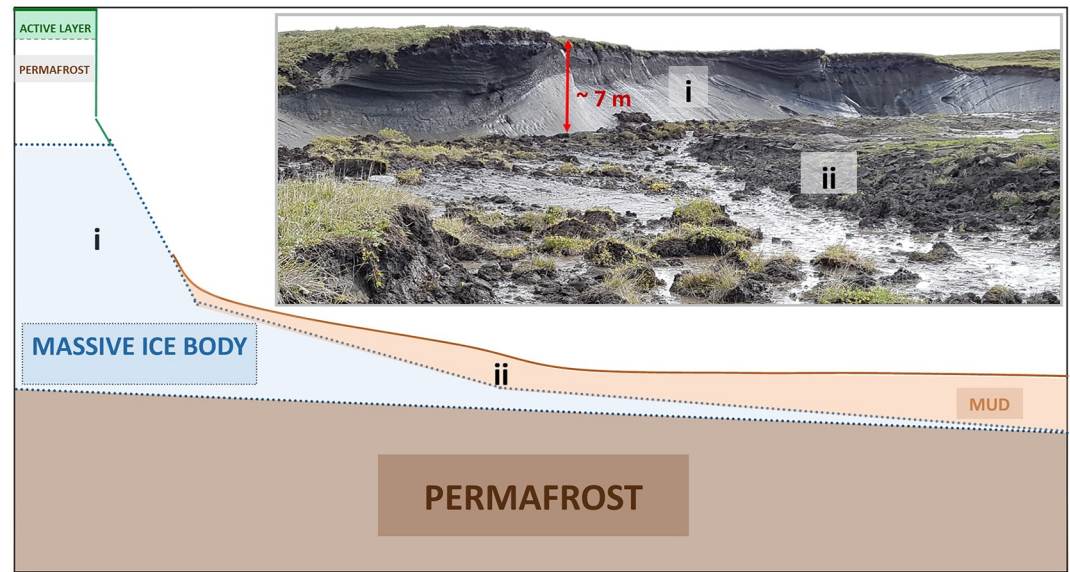


**Figure 1.** Schematic diagram with the main Retrogressive Thaw Slumps (RTS) features and an inset image of these features from a RTS on Pelly Island in 2017, featuring (i) the headwall and (ii) the slump floor.

water flow along a massive ice body or layer of ice rich permafrost. Active thaw slumps are traditionally characterized by a distinctive “C” shaped scar zone containing two main elements (Figure 1);

- i. A headwall consisting of an active layer, ice-poor permafrost and an exposure of massive ice—the ablation of which drives the back wasting of the RTS
- ii. A low angled slump floor, where thawed permafrost material from the headwall combines with meltwater to form a muddy mixture which flows downslope

RTS initiation occurs when the ice rich permafrost or massive ice is exposed to surface energy fluxes, causing ablation of the ice and upslope progression of the headwall. The exposure can occur due to a variety of reasons, such as shoreline retreat in coastal regions, riverbank erosion inland, gullyng from snowmelt and rainfall or penetration of the active layer (the seasonally thawed surface layer of permafrost) to the ice rich layers below.

The areal extent of RTS affected terrain has undergone a dramatic increase in the last two decades across the ice rich morainial landscapes of the western Canadian Arctic (Kokelj et al., 2015; Lantuit et al., 2012; Lewkowicz & Way, 2019; Ramage et al., 2018) where it is now believed to be the dominant driver of geomorphic change in the region (Segal et al., 2016). While some studies have had success in linking RTS activity (through measurements of headwall retreat (HWR) or RTS growth) to environmental variables, such as thawing degree days (Swanson & Nolan, 2018; Ward Jones & Pollard, 2021), the majority of these attempts have proven inconsistent and typically suited to a narrow range of meteorological and geomorphic conditions (Heginbottom, 1984; Lewkowicz, 1987; Robinson, 2000; Ward Jones et al., 2019; Zwieback et al., 2018). Similarly conflicting results appear when examining factors such as slope, orientation and headwall height (Lewkowicz, 1987; Ramage et al., 2017; Swanson & Nolan, 2018; Wang et al., 2009, 2016; Ward Jones et al., 2019). These inconsistent results suggest that there may be further in situ controls that play an important role in the activity of RTSs. Across these studies just mentioned, various factors such as the thickness of exposed massive ice in the headwall, the overburden (the soil layer overlying the massive ice body) thickness, and terrain variability (which can also affect the massive ice and overburden thicknesses) have been offered as potential confounding variables. As such, knowledge of how the massive ice and overburden thicknesses vary across RTS dominated landscapes may offer some potential avenues to better constrain the rates of RTS growth, variations in HWR within a single thaw slump or slump complex, and potentially their initiation and quiescence.

The recent increase in lidar use (Obu et al., 2016; Ramage et al., 2017) and Structure from Motion-Multiview Stereo (SfM-MVS) derived digital elevation models (Cunliffe et al., 2019; Swanson & Nolan, 2018; Westoby et al., 2012) have provided new opportunities to better measure ground surface topography and change. However, detection and mapping of subsurface massive ice and overburden variability remains primarily limited to visual observations of their exposures along cliffs and headwalls, sporadic borehole measurements and identification

of surface features that may act as proxy indicators for the presence of massive ice. Interpolation and extrapolation of these values to produce regional massive ice models (Couture & Pollard, 2017; Couture et al., 2018) may result in significant inaccuracies, especially on local scale, placing a limitation of estimates of carbon loss and management of vulnerable infrastructure. Only recently have new methods emerged for mapping massive ice non-invasively using passive seismic recordings (Lim et al., 2020). Here we present a site study consisting of inter-annual, high spatial resolution SfM-MVS data in combination with passive seismic monitoring of subsurface layering to address these critical problems.

## 2. Study Area

Peninsula Point is located within the Pingo National Park, 6 km southwest of Tuktoyaktuk, Northwest Territories, Canada (Figure 2). The regional landscape lies within the zone of continuous permafrost (with permafrost temperatures between  $-6^{\circ}$  and  $-7^{\circ}\text{C}$  (Burn & Kokelj, 2009)), is dominated by rolling hills with a maximum elevation of about 50 m, and thermokarst lake coverage of between 30% and 50% (Mackay, 1963). Surficial soils consist of various glaciolacustrine and glaciofluvial deposits, a result of its position at the northern edge of the Laurentide ice sheet at the end of the last glacial period (Mackay, 1971; Murton et al., 2005). The climate in the region is considered subarctic, with temperatures below freezing from October to late May, reaching a low of approximately  $-25^{\circ}\text{C}$  between December and March. Temperatures are typically above  $0^{\circ}\text{C}$  from late May to September, coinciding with the period when snow and sea ice cover are largely absent (Burn & Kokelj, 2009). The Peninsula Point island itself is characterized by a 2–10 m thick layer of clay rich diamicton, atop a massive ice body of between 5 and 20 m thickness, some of which lies below sea level. Below the ice lies a layer of deltaic sands (Mackay, 1963). The massive ice layer is understood to have formed as ground water, sourced from nearby receding glaciers, was forced toward an aggrading permafrost table less than 14,000 years BP (Mackay & Dallimore, 1992; Moorman et al., 1998). The site contains a range of massive ice exposures with different thicknesses, variable headwall heights and signs of polycyclic RTS activity (such as in the western segment of Figure 2c). Other areas also hint at signs of older RTS activity, although these are difficult to confirm objectively as the areas have stabilized and re-vegetated.

Shoreline retreat, HWR, massive ice exposures and RTSs dynamics at Peninsula Point have been monitored, at variable intervals, since 1935 (Mackay, 1986), allowing it to become a “type locality” for massive intra-sedimental ice in the western Canadian Arctic (Murton et al., 2005). These features make it an ideal site for assessing the role of massive ice and headwall properties on RTS activity.

## 3. Methods and Data

### 3.1. Remotely Sensed Imagery

High-resolution aerial imagery ( $1.8\text{ cm}^2$  at nadir) was captured during the summers of 2016, 2017 and 2018 using the DJI Phantom 4 drone. A total of between 600 and 1,000 useable aerial images were collected in each survey. Ten black and white markers were distributed throughout the site to use as ground control points. These were georeferenced using real-time kinematic differential global navigation satellite system to produce centimeter scale locational accuracy ( $\pm 10\text{ cm}$  horizontal,  $\pm 25\text{ cm}$  vertical). Drone images were processed using the SfM-MVS method to generate high-resolution DEMs and georegistered orthomosaics. SfM-MVS is a photogrammetric range imaging approach that allows for high resolution 2.5D surface reconstruction through the analysis of overlapping 2D images. Images can be captured using consumer grade digital cameras (Carrivick et al., 2016; Westoby et al., 2012), and can produce results with similar levels of accuracy to terrestrial laser scanners, but with a fraction of the cost (James & Robson, 2012; Westoby et al., 2018). The 2016 drone images were processed using Pix4D software (Pix4D-mapper, 2016). The remaining data were processed using Agisoft Photoscan 1.2.4© (Agisoft, 2016), with all point clouds finely co-registered using the CloudCompare (CC) software (CloudCompare v2.7.0, 2020).

#### 3.1.1. Model Co-Registration

The 2016-point cloud was chosen as the base model on which the other SfM-MVS models were registered, accuracy assessed and rates of HWR determined. Horizontal accuracy was calculated by comparing the position of discreet ground surface features across the 3 years. For 2017 and 2018, 10 distinct features were used for comparison, resulting in a root mean square error (RMSE) for 2017 of 0.12 m for  $X$ , and 0.14 m for  $Y$  and an RMSE for 2018 of 0.15 m in  $X$  and 0.11 m in  $Y$ .

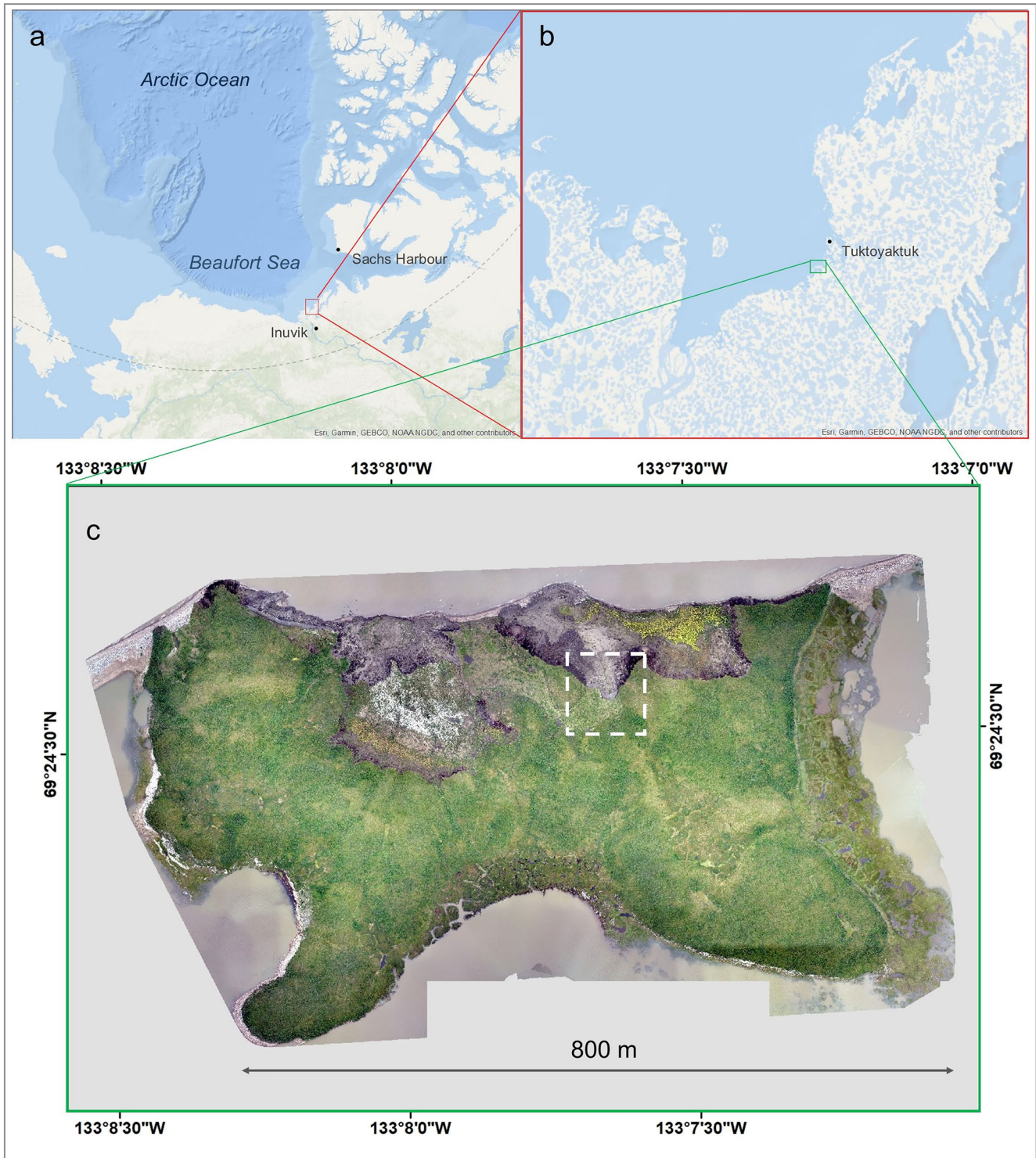


**Figure 2.** Location of the field site, Peninsula Point. Panel (a) is the location within the Arctic Ocean. Panel (b) shows it within the Tuktoyaktuk Peninsula Region and panel (c) shows a drone-based orthomosaic of the Peninsula Point site itself with the dashed box indicating the detailed monitoring area.

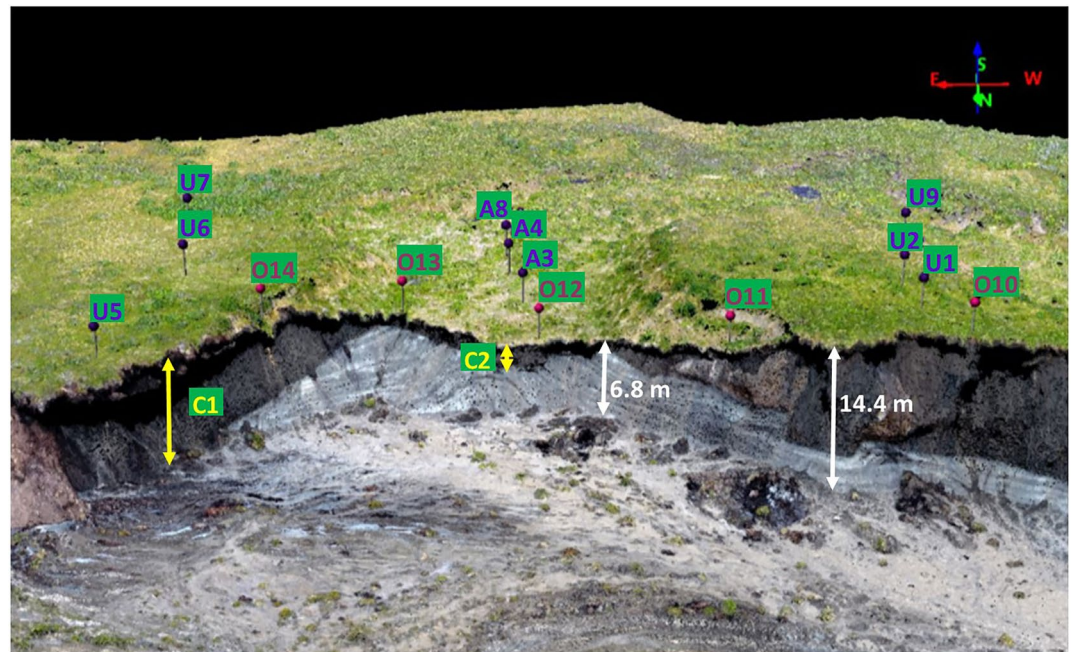


**Figure 3.** Passive seismic measurement and observations points. The measurement locations are labeled “U” for undisturbed and “A” for active ground. Calibration points are labeled “C” and visual observation points labeled “O”.

Vertical accuracy was assessed using eight 25 m long elevation profiles in the undisturbed terrain. For 2017 and 2018 the vertical RMSEs were 0.10 and 0.20 m, respectively.

### 3.2. Massive Ice Elevation and Overburden Thickness

Determination of the depth to massive ice followed to process of Lim et al. (2020), but is briefly described here. Seismic noise is present throughout the lithosphere and can be used to gather data on subsurface properties. Monitoring of this noise has been used in various geological settings to determine features such as the depth of subsurface strata or the different seismic wave velocities of the buried rock and soil (Cultrera et al., 2012; Scheib, 2014; Tallett-Williams et al., 2016). Subsurface strata exhibit differences in the amplitude of their vertical and horizontal motions. This occurs due to impedance contrasts between layers and differences in the shear and compressional wave velocities of the materials. This allows for the data to be processed using the H/V (horizontal to vertical) ratio method (Nakamura, 1989) to identify the natural resonance frequencies of the subsurface strata. For a simple two-layer system (in this case the two layers are overburden and massive ice), the resonance frequency can be used in the following formula to calculate the depth of the layer boundary:

$$f_r = \frac{V_s}{4h}$$

Where  $f_r$  is the resonance frequency,  $V_s$  the shear wave velocity and  $h$  is the depth.

In August 2017, passive seismic data were collected in nine locations on Peninsula Point, as three separate North to South transects with three measurements each, all using the Tromino<sup>®</sup> device (<http://moho.world/en/tromino/>). One transect was along a low-ground segment that had recently been affected by RTS activity and where the active layer extended to the surface of the massive ice (indicated with “A” label in Figure 3). Two further transects were along undisturbed high ground to both the east and west of the first transect that contained permafrost layers between the ground surface and the massive ice (indicated with “U” labels in Figure 3). A further five massive ice height measurements were taken from headwall exposures (indicated with “O” labels in Figure 3).

Processing of the seismic signal allowed for the  $f_r$  to be calculated but to determine the depth to the massive ice it was necessary to calculate the  $V_s$  of the overburden layers. This was achieved by selecting two measurement points near the headwall edge, one for the low ground without permafrost and one for the high ground that

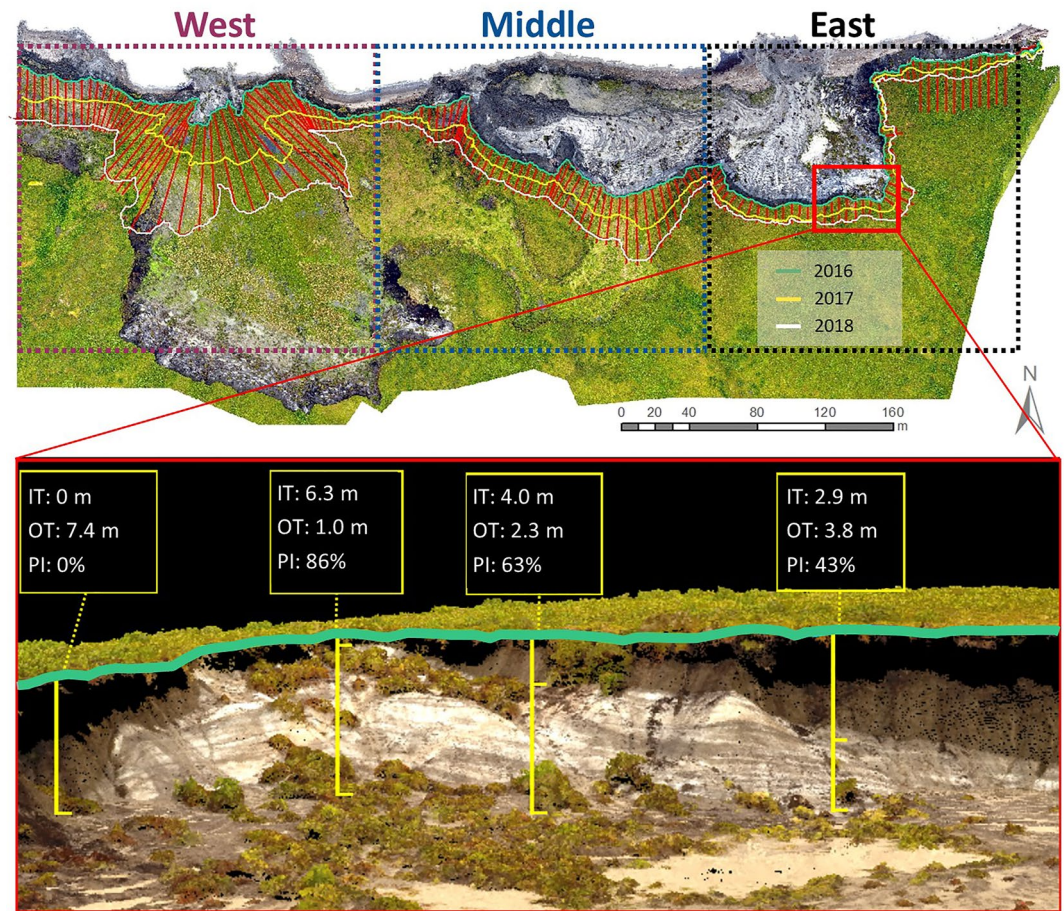


**Figure 4.** 2016 Structure from Motion-Multiview Stereo model in plan view with the headwall positions color coded by year and split into east, middle and west (top) and a detailed example of the massive ice thickness, overburden thickness and proportion of massive ice headwall measurements for a small, variable section (bottom).

contained permafrost. The observable depth to massive ice near these measurement points provided  $h$  values, while the H/V processing method provided the  $f_r$  values. By using these control measurement points, the  $V_s$  for the two overburden layers could then be calculated. For the high ground, this produced a  $V_s$  of 1059.38 m s<sup>-1</sup>, which was then be applied to the five other high ground points to determine their respective depths to the massive ice surface. For the low ground section, doing the same produced a  $V_s$  of 213.8 m s<sup>-1</sup>, a significantly slower velocity, due to the greater water content of the thawed soil. This value was then applied to the two other low-ground segments to calculate their respective massive ice depths. Finally, a continuous massive ice surface layer was then created using the inverse distance weighted interpolation within ArcGIS 10.3.

### 3.3. Active Headwall Properties

Using the SfM-MVS point clouds for 2016, 2017 and 2018, active headwalls were digitized and categorized based on the ice thickness (IT), overburden thickness and proportion of massive ice (PI) visible from their exposures. This resulted in three separate headwall lines in each year, amounting to nine in total. An example of the headwall positions in each year and extra detail of the measurements from a small section is provided in (Figure 4). Transects were added at 5 m intervals, perpendicular to the direction of HWR, where headwall properties were measured for each year. Headwall retreat rates were also assessed by manually measuring the change in headwall position along each transect for each year, producing rates for 2016 to 2017, and 2017 to 2018. Transects that contained no clear exposures of massive ice in any of the 3 years were excluded from the numerical analysis and correlations. This reduced the number of useable transects from 163 to 128.

**Table 1**

*Overall Stats in Terms of Headwall Retreat, Ice Thickness, Overburden Thickness and Proportion of Massive Ice in Headwall Exposures on Peninsula Point in 2016, 2017 and 2018, With Standard Deviations in Brackets*

	HWR (m)	IT (m)	OT (m)	PI
2016: East	N/A	2.9 (1.9)	5.8 (3.0)	37% (27%)
2016: Middle	N/A	2.2 (1.2)	7.4 (4.5)	30% (23%)
2016: West	N/A	0.4 (0.5)	2.6 (0.9)	15% (18%)
2016: Mean	N/A	1.7 (1.6)	5.1 (3.7)	26% (24%)
2017: East	7.3 (1.8)	0.5 (1.5)	6.6 (2.3)	9% (25%)
2017: Middle	11.4 (4.4)	2.4 (2.0)	9.3 (4.4)	24% (26%)
2017: West	16.7 (9.4)	0.9 (0.8)	2.3 (0.9)	24% (22%)
2017: Mean	12.5 (7.5)	1.3 (1.6)	5.8 (4.2)	21% (25%)
2018: East	3.3 (2.3)	0.2 (0.8)	6.5 (2.0)	5% (17%)
2018: Middle	9.9 (3.7)	0.4 (1.1)	9.4 (3.7)	9% (22%)
2018: West	23.8 (15.8)	1.7 (0.9)	2.2 (0.6)	27% (12%)
2018: Mean	13.9 (13.4)	0.9 (1.2)	5.7 (4.0)	21% (24%)
Mean	13.2 (9.4)	1.3 (1.0)	5.5 (3.8)	22% (18%)

*Note.* HWR values are for 2016–2017 (2017), 2017–2018 (2018) and the 2016–2018 (Mean) (note that HWR rates are not available for 2016 as it was the first year of measurement).

### 3.4. 3D Layering

Using a combination of the surface elevation data derived from the SfM-MVS models, ALD measurements and the massive ice surface model from Section 3.2, a 3D layer model was created for the middle portion of Peninsula Point and 12 transects extracted from it in order to create a fence diagram—allowing for a comparison and visualization of surface features with internal overburden thickness and massive ice elevation.

## 4. Results

### 4.1. Active Headwall Analysis

#### 4.1.1. Headwall Properties and Retreat Rate Variations

The average HWR rate increased from 12.5 m from 2016 to 2017, to 13.9 m from 2017 to 2018, with an average of 13.2 m from 2016 to 2018. The east and middle sections (Figure 4) experienced HWR rates of 7.3 and 11.4 m respectively between 2016 and 2017, reducing to 3.3 and 9.9 m respectively for 2017 to 2018. In contrast, the west recorded a mean HWR of 16.7 m for 2016 to 2017, increasing to 23.8 m for the 2017 to 2018 period. The HWR rates over the 2 years along individual transects ranged from 1.6 m a<sup>-1</sup> to 41.9 m a<sup>-1</sup>. Changes in the headwall properties followed a similar pattern to the HWR rates. The IT and PI values decreased overall in the east and middle segments, while increasing in the west. The opposite is true of overburden thickness, which increased in the east and middle, and decreased in the west (Table 1).

#### 4.1.2. Massive Ice Thickness and Headwall Retreat

IT values in 2016 and 2017, and the mean IT across all 3 years, produced weak and variable (Pearson) correlations with HWR rates, between  $-0.28$  and  $+0.20$  (Table 2). IT in 2018 produced significant positive correlations with HWR across all timespans, with an overall correlation coefficient of  $+0.47$  between the 2018 IT and the 2016 to 2018 HWR rates ( $p < 0.05$ ). However, no statistically significant differences were noted on the influence of the IT categories in 2018 (no ice, 0–2 m, 2–4 m) on the mean HWR rates (Figure 5a).

**Table 2**

*Correlation Coefficients Between the Headwall Properties, Ice Thickness, Overburden Thickness and Proportion of Massive Ice*

		Headwall retreat		
		2016–2017	2017–2018	2016–2018
Headwall Properties	2016 IT	<b><i>-0.20</i></b>	<b><i>-0.28</i></b>	<b><i>-0.28</i></b>
	2017 IT	<b><i>0.20</i></b>	0.15	<b><i>0.19</i></b>
	2018 IT	<b><i>0.33</i></b>	<b><i>0.47</i></b>	<b><i>0.47</i></b>
Average IT		0.13	0.11	0.13
Average OT	2016 OT	<b><i>-0.42</i></b>	<b><i>-0.45</i></b>	<b><i>-0.49</i></b>
	2017 OT	<b><i>-0.41</i></b>	<b><i>-0.47</i></b>	<b><i>-0.50</i></b>
	2018 OT	<b><i>-0.38</i></b>	<b><i>-0.48</i></b>	<b><i>-0.50</i></b>
Average OT		<b><i>-0.42</i></b>	<b><i>-0.49</i></b>	<b><i>-0.52</i></b>
Average PI	2016 PI	0.08	0.01	0.04
	2017 PI	<b><i>0.43</i></b>	<b><i>0.41</i></b>	<b><i>0.46</i></b>
	2018 PI	<b><i>0.42</i></b>	<b><i>0.59</i></b>	<b><i>0.58</i></b>
Average PI		<b><i>0.42</i></b>	<b><i>0.46</i></b>	<b><i>0.49</i></b>

*Note.* Bold values are significant to  $p < 0.05$ , while those bold and italicised are significant at  $p < 0.01$ .

#### 4.1.3. Overburden Thickness and Headwall Retreat

The thickness of the exposed overburden in all years produced statistically significant negative correlations with HWR rates, the strongest being between the average overburden thickness across all 3 years and the average HWR from 2016 to 2018 ( $-0.52$ ). Examining the mean overburden thickness across all 3 years, the influence over HWR rates can be split into three broad categories; below 2 m, 2–4 m and above 4 m. An average overburden thickness of 0–2 m is associated with an average HWR of 27.3 m a<sup>-1</sup>, 2–4 m overburden thickness averages 14.8 m a<sup>-1</sup>, while all higher categories average between 7.7 and 9.0 m a<sup>-1</sup> (Figures 5b and 6b).

#### 4.1.4. Proportion of Massive Ice and Headwall Retreat

As with the IT, the PI in 2016 had no significant influence over the subsequent HWR rates. Statistically significant correlations were present between the PI in 2017 and HWR rates, but the strongest correlations occurred with the 2018 PI values. The correlation between the 2018 PI and the 2016 to 2018 HWR rate is  $+0.58$  ( $p < 0.05$ ) and with the 2017 to 2018 HWR rate is

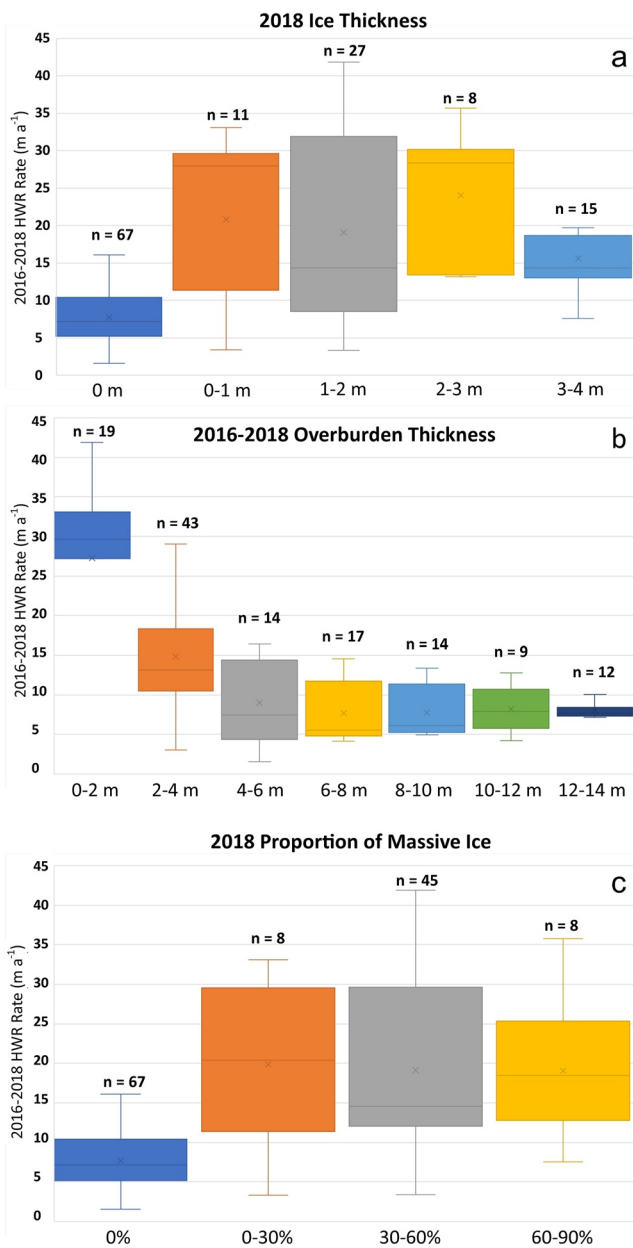


**Figure 5.** Plots depicting the relationship between the 2016 and 2018 headwall retreat rates and (a) Ice thickness in 2018, (b) average overburden thickness across all 3 years and (c) proportion of massive ice in 2018. Boxes represent 75% variance and whiskers show the maximum and minimum values.

+0.59. However, as with the IT metric, the correlation is non-linear, influenced heavily by the slow HWR associated with the 0% PI category, while any PI above 0%, irrespective of how high or low, are associated with faster rates of HWR (Figures 5c and 6c).

#### 4.1.5. In Situ Controls on Headwall Retreat Rates

To further refine the relationship between the HWR rates and both the overburden thickness and IT, we separated the observations based on two distinct criteria—(a) a mean overburden thickness below 4 m and (b) the presence of massive ice inland of the headwall, regardless of its thickness or the proportion of the headwall for which it accounted. When both criteria are met, the average HWR rate is 20.4 m a<sup>-1</sup>, while all other headwalls retreat at an average of 9.5 m a<sup>-1</sup> (Figure 7).

#### 4.2. 3D Layer Model

Using transects extracted along the black lines in Figure 8a, the fence diagram in Figures 8b–8e was created. The middle portion of the model shows a high elevation ice surface, with a thin overburden and an active layer extending down to the massive ice, with little change extending inland. The overburden thickness averages 2.5 m, with a  $\sigma$  of 0.6 m (Figures 8b and 8d). The high ground to the east contains an average overburden thickness of 9.0 m and a  $\sigma$  of 1.9 m. The ice and ground surface slowly decrease in elevation inland, resulting in no significant cross-shore trend in overburden thickness (Figure 8e). The high ground to the west contains both the most variability in ice surface elevation and overburden thickness. The average overburden thickness is 10.7 m with a  $\sigma$  of 2.5 m. It contains a large overburden thickness range, from 5.3 to 14.7 m, and contains a distinct bowl-like depression where the ice surface is close to sea level. These substantial variations in massive ice elevation are not reflected in the surface topography (Figure 8c).

##### 4.2.1. Massive Ice Model Validation

HWR from 2017 to 2018 provides a means of validating the accuracy of the massive ice model by comparing the modeled ice surface elevation with the resultant 2018 headwall exposures. The trends in IT and overburden thickness exposed in the headwalls from 2016 to 2017 can be seen in Figure 9. The IT increased and overburden thickness decreased in the middle and western segments, while the opposite trend occurred in the east. The massive ice elevation model predicts a continuation of a high elevation massive ice and thin overburden thickness in the middle and a reduction in IT and overburden thickness in the east. Ice in the west is modeled to dip steeply inland with a large reduction in the PI, counter to the 2016–2017 trend. The exposures present in 2018 in Figure 9 allow for a comparison between the predicted massive ice surface (white dashed line) and the actual massive ice surface.

The model accurately predicted the inland ice surface elevation pattern, with a maximum observed difference of just 1.4 m. The western segment was modeled to dip by between 2° and 18° from the 2017 position but, based on the resultant headwall exposures (and lack thereof), the actual angles are estimated to have been between 10° and 30°. Some ice may have been hidden under mud just behind the headwalls and, where the ice is below the base of the headwall, its elevation cannot be determined from visual observations. These factors may have increased the difference in observed and modeled ice elevation.

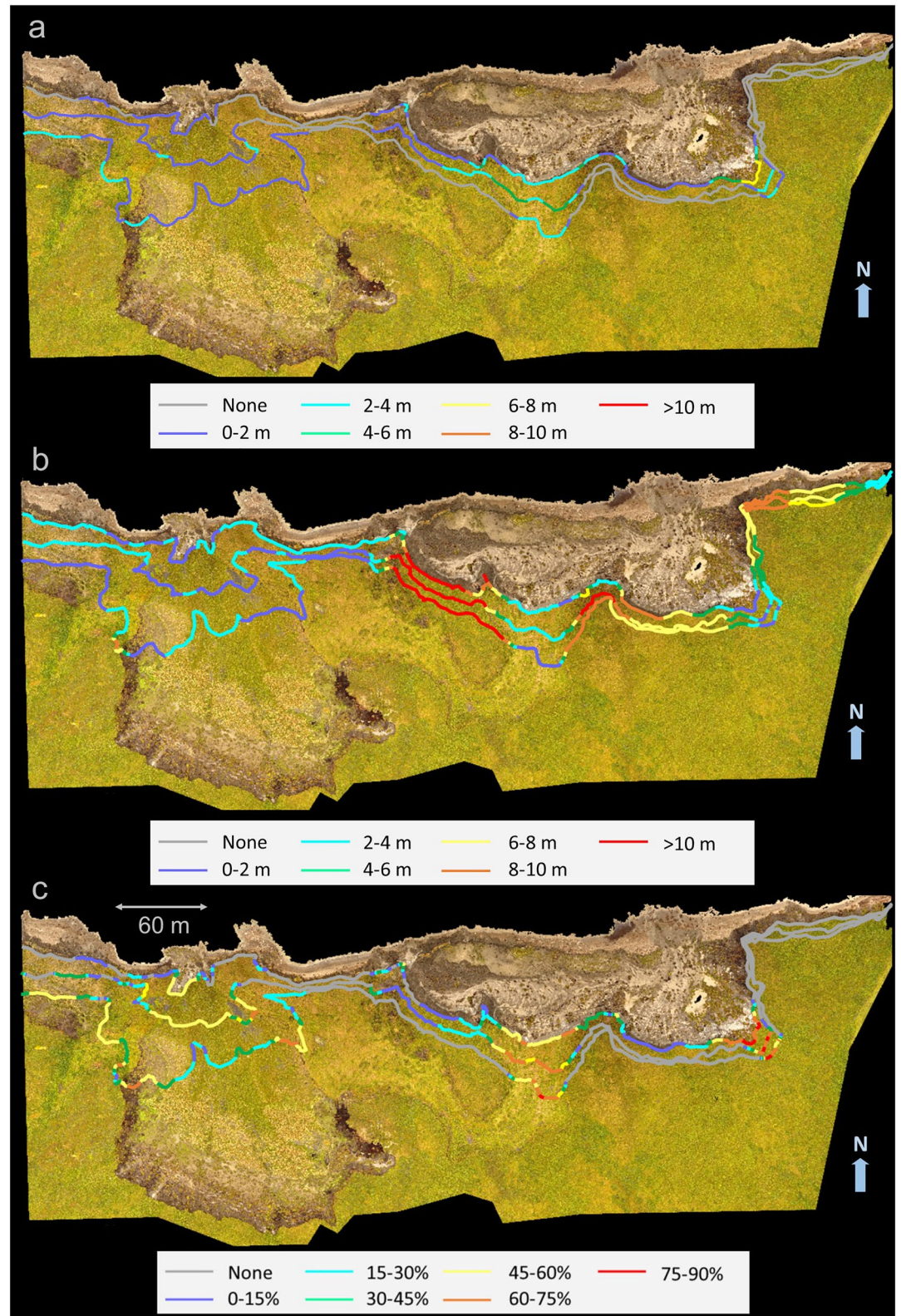


**Figure 6.** Headwall lines in 2016, 2017 and 2018, digitized and color coded based on (a) ice thickness, (b) overburden thickness and (c) proportion of massive ice, and overlaid on a 2016 image. These highlight the distribution of headwall properties and their relationship to headwall retreat.

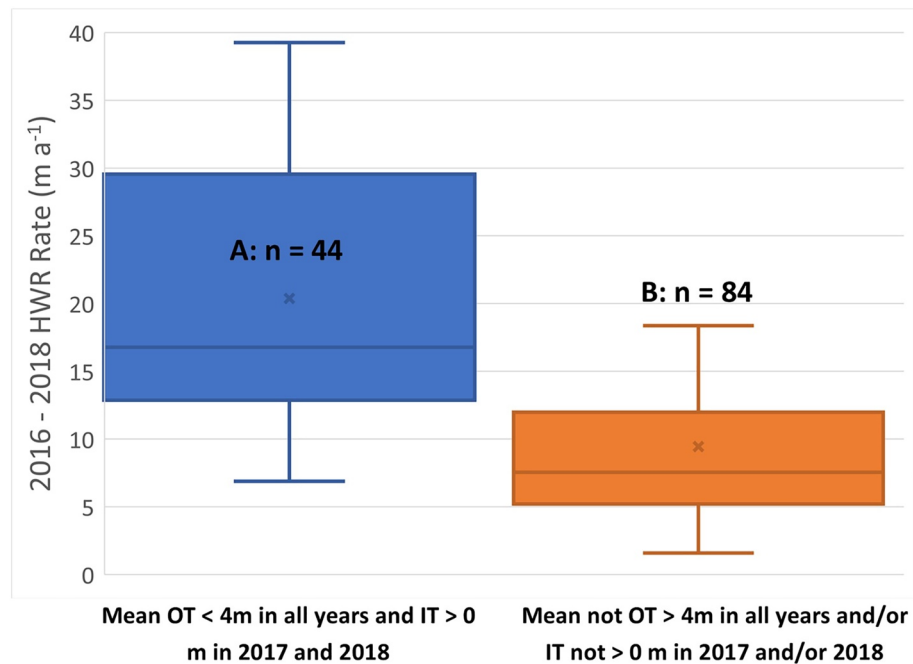


**Figure 7.** The headwall retreat rates along the transects on Peninsula Point are twice as fast on average and more variable where (a) the average overburden thickness remains below 4 m and ice is present in 2017 and 2018 compared to (b) where these criteria are not met.

## 5. Discussion

### 5.1. Passive Seismic for Subsurface Layer Mapping

The presence and surface elevation of massive ice inland of the headwall, and thus the overburden thickness and IT also, cannot be determined easily without costly and invasive borehole measurements. Similarly, the presence of water rich active layers, and especially thawed soils reaching the massive ice, attenuate the signals from ground penetrating radar, reducing their effectiveness in these environments (Campbell et al., 2018). Passive seismic measurements now offer the potential to spatially map these features away from the cliff face and hence produce more accurate characterizations of existing conditions and potentially improve forecasts of HWR rates.

The massive ice surface model on Peninsula Point was shown to accurately represent the internal surface variations of the massive ice body and overburden thickness, demonstrating the efficacy of the passive seismic device and analysis method presented. The layer model also revealed variability not detectable from headwall exposures, their extrapolations or surface features, such as the rapid reduction in ice surface elevation and the bowl-like depression in the western section (Figure 8c). Using the 2018 headwall exposures as validation, a maximum difference of 1.4 m was found between the modeled and observed massive ice surface. When comparing the headwall exposures closest to the passive seismic measurement points, where the ice surface is not modeled below the headwall base, the layer boundaries were accurate to within 0.5 m. These validations demonstrate that the technique can be used to accurately detect subsurface layering depth and suggest that a greater density of measurements may be required to accurately capture the fine scale variations.

Knowledge of the massive ice variability and overburden thickness have been noted as critical to understanding the geomorphic response of Arctic landscapes to climate change and other anthropogenic disturbances (Pollard, 1990; Segal et al., 2016). On Banks Island, observations show that there has been a 60-fold increase in RTS numbers between 1984 and 2015 (Lewkowicz & Way, 2019). It has been suggested that a thin overburden, as little as 1 m in places (Lakeman & England, 2012), is a significant contributor to the observed landscape sensitivity on Banks Island. This thin overburden thickness exacerbates the relatively slow warming trend by allowing the surface energy to more easily reach the near surface massive ice, thus triggering the formation of new RTSs (Rudy et al., 2017; Segal et al., 2016). This highlights the need for locally detailed maps of overburden thickness and massive IT variability in vulnerable areas, to aid in determining the likelihood of rapid geomorphic

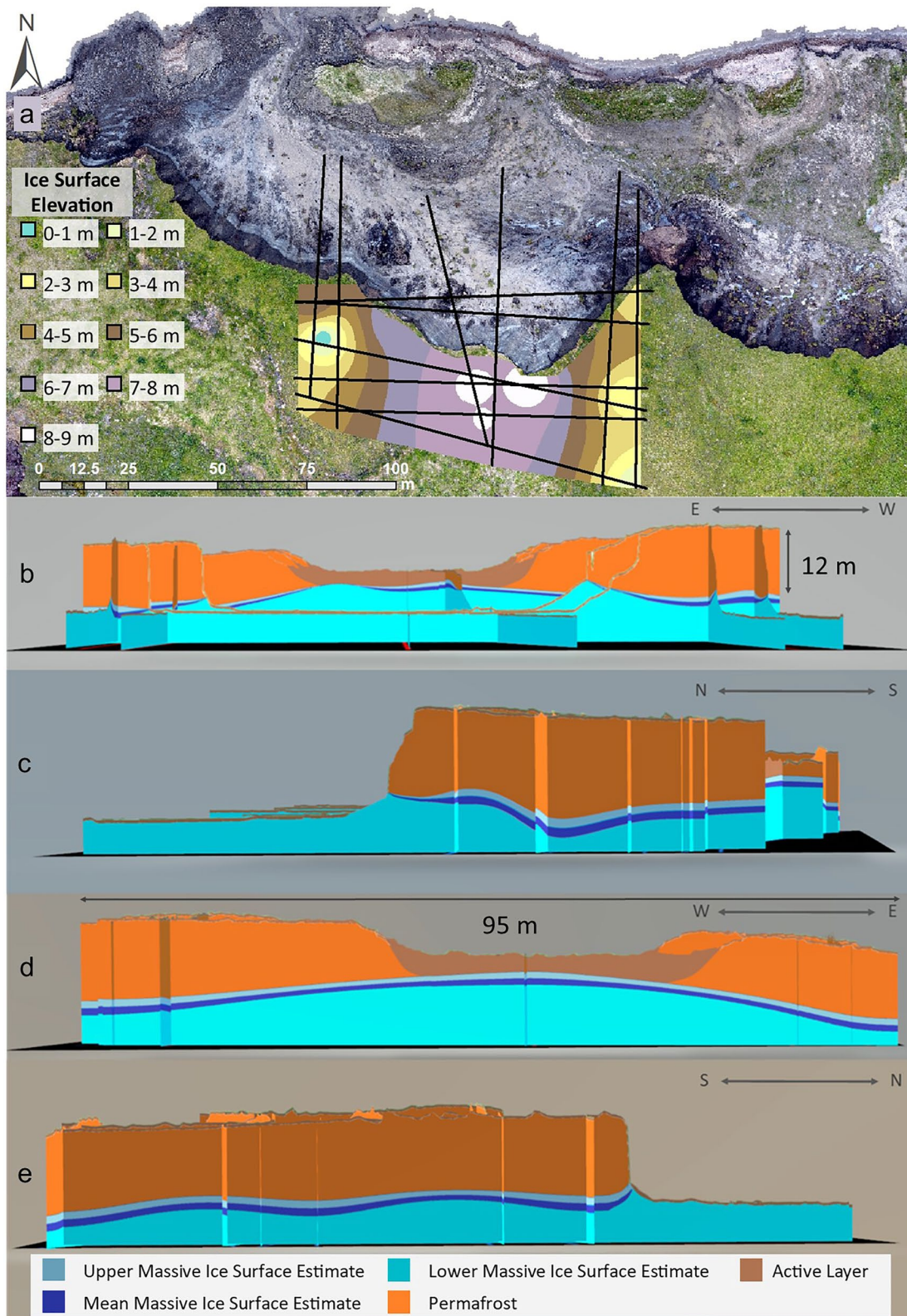


**Figure 8.** Section (a) shows a plan view of the location of the massive ice surface model (elevation relative to local sea level) within Peninsula Point. The black lines in section a represent the locations of the panels that constitute the fence diagram, which is shown in different perspectives from section (b) through to (e).

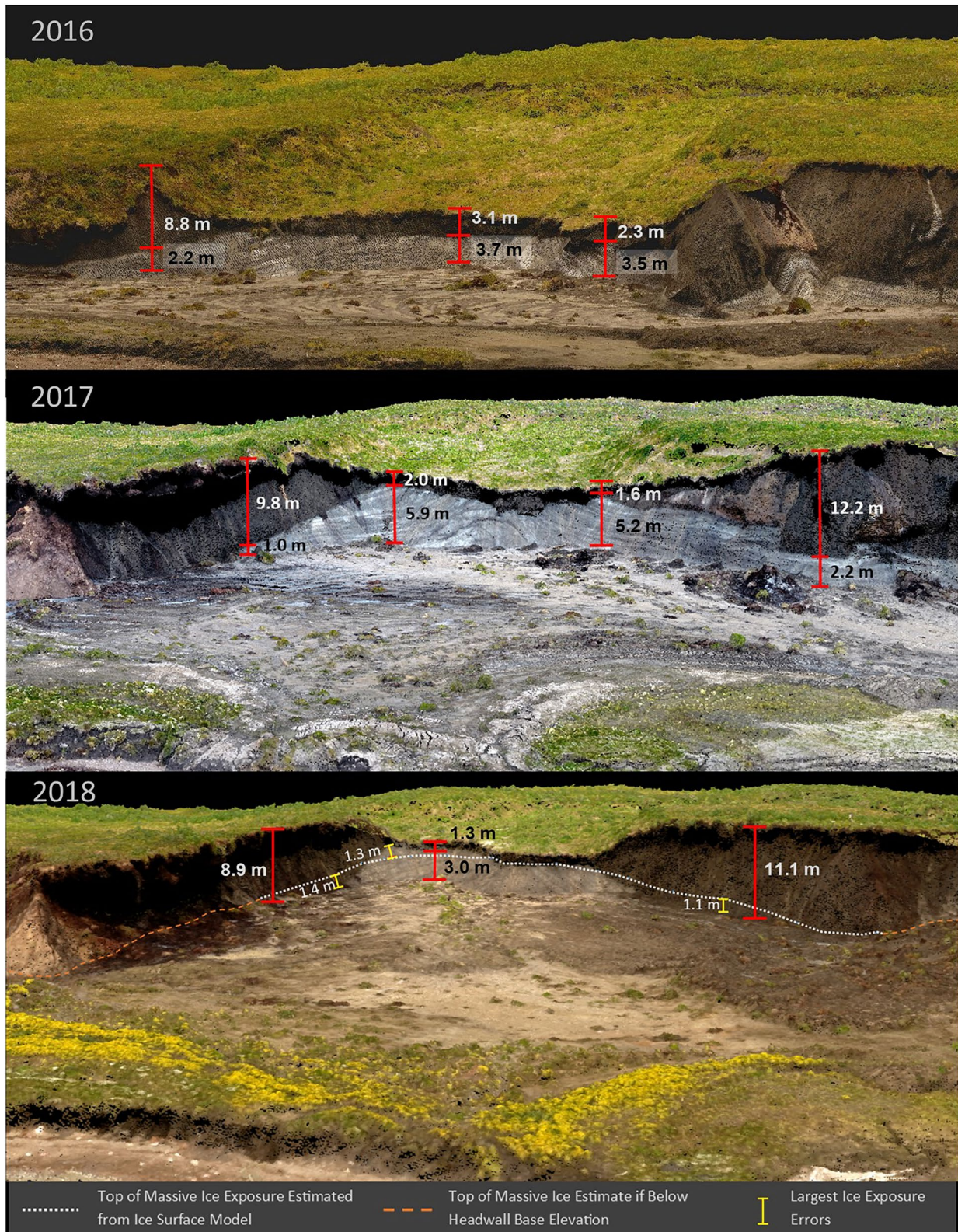


**Figure 9.** Examples of ice thickness and overburden thickness observations for the same location in all 3 years. The trends from 2016 to 2017 for the middle and western segments reversed in 2017–2018, as predicted by the modeled massive ice height (white dash).

disturbances under continued warming in the near future—an area in which passive seismic monitoring can play a key role.

While some studies have identified the terrain controls that lead to the formation of RTSs (Ramage et al., 2017) the ability to predict when a RTS can become active, re-activate (for polycyclic RTSs) or stabilize, has generally been lacking. With this study we show that by mapping the depth and distribution of massive ice through passive seismics, areas with a high risk of RTS formation or other related forms of rapid geomorphic disturbance can be identified. Moreover, in the case of coastal settings, this study highlights that maps of massive ice variability combined with the local shoreline retreat rate may allow for predictions of when the massive ice body will be exposed and trigger RTS formations. Further, in regions with active RTSs, mapping of massive ice and overburden variability may allow predictions of RTS stabilization and improved understanding of their polycyclic activity patterns (Lantuit et al., 2012).

It has been shown that volumetric losses from mass wasting in ice rich permafrost can be several times greater than mass loss arising from shoreline retreat alone (Günther et al., 2015; Lim et al., 2020). More accurate models of the relative proportions of massive ice and overburden thickness can allow for improved estimates of future soil losses, and thus better constrained predictions of carbon, nutrient and pollutant fluxes in areas susceptible to RTS activity. They also have important implications for determining future levels of thaw subsidence. Passive seismic mapping of massive ice could be an element of infrastructure planning in ice-cored permafrost terrain. This could play a role in determining the susceptibility of soils to thaw subsidence, a significant contributor toward the cost of building and infrastructure maintenance across permafrost terrain (Clement et al., 2013; Couture & Pollard, 2017; Couture et al., 2018; Jones et al., 2008).

## 5.2. Headwall Factors Governing Short-Term HWR Rates

While some studies have successfully used thaw indices and simple geometric models to explain rates of HWR and RTS growth (Swanson & Nolan, 2018; Ward Jones & Pollard, 2021), the results from most studies have been spatially and temporally inconsistent, with several authors citing a lack of locally accurate terrain data, with a paucity of massive ice and overburden thickness variability acting as a significant constraint (Heginbottom, 1984; Lewkowicz, 1987; Robinson, 2000; Zwieback et al., 2018). Here, we note two dominant in situ controls upon HWR on Peninsula Point. First, a persistent exposure of massive ice inland of the current headwall position, regardless of its thickness, and second, an average overburden thickness of under 4 m. Along transects where these criteria were met on Peninsula Point, HWR rates were more than twice as fast as otherwise. It appears that on Peninsula Point the absolute thickness and the proportion of the headwall that consists of massive ice play little role in determining the HWR rates. Rather, the presence of massive ice allows for the initiation of HWR, with the resulting rate of retreat being largely dictated by whether the overburden thickness is above or below 4 m. While these metrics may vary depending on site conditions (removal of thawed material, soil ice content, slope, elevation, etc.), examination of similar metrics in other RTS dominated regions may better contextualize the factors governing local HWR rates.

There is also clear evidence of terrain on Peninsula Point that has previously been affected by RTS activity, such as the large scar zone that's mainly at the back of the western segment (Figure 4). There are also regions that are unaffected and others where it's not completely clear whether they had been affected by previous RTS activity or not. Both affected and unaffected terrain show both some of the fastest and some of the slowest HWR rates across the site. While previous phases of thaw slumping may exert an influence on subsequent HWR rates through alterations of the ground thermal regimes (Zwieback et al., 2020), this research suggests that it may also influence subsequent HWR rates through their alteration of the massive ice and overburden thickness. Where they reduce the overburden thickness while maintaining an exposure of massive ice—they create conditions that allow for faster HWR rates. However, where they reduce or exhaust massive ice exposures, they can potentially slow subsequent HWR rates. As such, the influence they exert on future retreat rates may be through changing the thickness of the massive ice and overburden layers.

In the western portion of Peninsula Point, 16 transects contained no visible exposures of massive ice in 2016 (Figure 6a). However, 11 of those transects experienced HWR >10 m between 2016 and 2017, four of which exceeded 20 m. Had passive seismic monitoring been carried out in this region in 2016, it may have been possible to identify the region as having the requisite layering (massive ice and thin overburden) to produce rapid

rates of HWR once the massive ice was exposed. As such, passive seismic monitoring provides the potential to better predict and therefore mitigate against the dramatic geomorphic changes that occur in ice-cored terrain and highlights the need to detect and map massive ice variability to identify areas where new RTSs are likely to develop. With maps of overburden and massive ice variability inland of the headwall, it may also be possible to anticipate when the massive ice will no longer be exposed and the overburden layer will grow, allowing the rapid slowing or stabilization of RTSs to be more easily predicted.

## 6. Conclusion

Passive seismic monitoring has been shown to be an effective tool for detecting overburden thickness and massive ice surface variability. The resulting models showed variations in massive ice not apparent from headwall exposures or surface topographic features, and the opposite of those inferred from simple extrapolations of headwall exposures.

Overburden thickness and massive IT were found to exert a significant control over short term HWR rate variability from 2016 to 2018. Where the overburden thickness remained below 4 m and massive ice was present inland of the headwalls, HWR rates were more than twice as fast the headwalls that did not meet these criteria that is, headwalls that had an overburden greater than 4 m and/or did not maintain a massive ice exposure inland of their current position.

This research brings into focus the need for accurate data on massive ice and overburden thickness in order to understand the spatial and temporal variability in RTS activity. Better knowledge of massive ice variability can contribute to improved understanding of permafrost coastal dynamics, such as rates of shoreline retreat and volume loss. These findings have the potential to provide more accurate estimates of nearshore carbon and sediment fluxes and to improve assessments of the susceptibility of local landscapes to rapid geomorphic changes. We emphasize the need for widespread testing of these headwall metrics and passive seismic monitoring to ensure their efficacy and robustness across different ice-cored permafrost terrains.

## Data Availability Statement

All field and analysis data are available from Zenodo at <https://doi.org/10.5281/zenodo.4770736> (Hayes et al., 2021). The software used for the SfM modeling is Pix4Dmapper, which can be downloaded via (<https://www.pix4d.com/product/pix4dmapper-photogrammetry-software>) (Pix4Dmapper, 2016) and Agisoft Photoscan 1.2.4 (now called metashape) which can be downloaded via (<https://www.agisoft.com/downloads/installer/>) (Agisoft, 2016). For closely aligning the point clouds, CloudCompare 2.7.0 was used and can be downloaded via (<https://www.danielgm.net/cc/>) (CloudCompare v2.7.0, 2020).

## References

- Agisoft PhotoScan Professional, Version 1.2.4. (2016). Agisoft PhotoScan professional, version 1.2.4. [Software]. Agisoft Photoscan. Retrieved from <http://www.agisoft.com/downloads/installer/>
- AMAP. (2017). *Snow, Water, Ice and Permafrost in the Arctic (SWIPA)*. Arctic Monitoring and Assessment Programme (AMAP), (Vol. 269). *xiv* +.
- Biskaborn, B. K., Smith, S. L., Noetzi, J., Matthes, H., Vieira, G., Streletskiy, D. A., et al. (2019). Permafrost is warming at a global scale. *Nature Communications*, 10(1), 264. <https://doi.org/10.1038/s41467-018-08240-4>
- Burn, C. R., & Kokelj, S. V. (2009). The environment and permafrost of the Mackenzie delta area. *Permafrost and Periglacial Processes*, 12, 53–68. <https://doi.org/10.1002/ppp.655>
- Campbell, S., Affleck, R. T., & Sinclair, S. (2018). Ground-penetrating radar studies of permafrost, periglacial, and near-surface geology at McMurdo Station, Antarctica. *Cold Regions Science and Technology*, 148, 38–49. <https://doi.org/10.1016/j.coldregions.2017.12.008>
- Carrivick, J. L., Smith, M. W., & Quincey, D. J. (2016). *Structure from motion in the geosciences*. John Wiley & Sons.
- Clement, J. P., Bengtson, J. L., & Kelly, B. P. (2013). Managing for the future in a rapidly changing Arctic. A report to the President. In *A report to the President. Interagency Working Group on Coordination of Domestic Energy Development and Permitting in Alaska* (D. J. Hayes, Chair) (p. 59).
- CloudCompare v2.7.0. (2020). CloudCompare v2.7.0 [GPL Software]. CloudCompare. Retrieved from <http://www.cloudcompare.org/>
- Collins, M., Knutti, R., Arblaster, J., Dufresne, J. L., Fichet, T., Friedlingstein, P., et al. (2013). Long-term climate change: Projections, commitments and irreversibility. In *Climate change 2013-the physical science basis: Contribution of working group I to the fifth assessment report of the intergovernmental panel on climate change* (pp. 1029–1136). Cambridge University Press.
- Comiso, J. C. (2006). Arctic warming signals from satellite observations. *Weather*, 61(3), 70–76. <https://doi.org/10.1256/wea.222.05>
- Couture, N. J., Irrgang, A., Pollard, W., Lantuit, H., & Fritz, M. (2018). Coastal erosion of permafrost soils along the Yukon Coastal Plain and fluxes of organic carbon to the Canadian Beaufort Sea. *Journal of Geophysical Research: Biogeosciences*, 123(2), 406–422. <https://doi.org/10.1002/2017JG004166>

## Acknowledgments

The authors would like to thank the members of NRCAN who provided invaluable data and assistance in the field. We express our gratitude to the Aurora Research Institute in Inuvik, and the community of Tuktoyaktuk. The research leading to these results has received funding from the European Union's Horizon 2020 project INTERACT, under Grant agreement No 730938 and also the NERC Arctic Office, without which this work would not have been possible. Open access funding provided by IReL.

- Couture, N. J., & Pollard, W. H. (2017). A model for quantifying ground-ice volume, Yukon Coast, Western Arctic Canada. *Permafrost and Periglacial Processes*, 28(3), 534–542. <https://doi.org/10.1002/ppp.1952>
- Cultrera, M., Antonelli, R., Teza, G., & Castellaro, S. (2012). A new hydrostratigraphic model of Venice area (Italy). *Environmental Earth Sciences*, 66(4), 1021–1030. <https://doi.org/10.1007/s12665-011-1307-2>
- Cunliffe, A. M., Tanski, G., Radosavljevic, B., Palmer, W. F., Sachs, T., Lantuit, H., et al. (2019). Rapid retreat of permafrost coastline observed with aerial drone photogrammetry. *The Cryosphere*, 13(5), 1513–1528. <https://doi.org/10.5194/tc-13-1513-2019>
- Fritz, M., Vonk, J. E., & Lantuit, H. (2017). Collapsing Arctic coastlines. *Nature Climate Change*, 7(1), 6–7. <https://doi.org/10.1038/nclimate3188>
- Günther, F., Overduin, P. P., Sandakov, A. V., Grosse, G., & Grigoriev, M. N. (2013). Short-and long-term thermo-erosion of ice-rich permafrost coasts in the Laptev Sea region. *Biogeosciences*, 10(6), 4297–4318. <https://doi.org/10.5194/bg-10-4297-2013>
- Günther, F., Overduin, P. P., Yakshina, I. A., Opel, T., Baranskaya, A. V., & Grigoriev, M. N. (2015). Observing Muostakh disappear: Permafrost thaw subsidence and erosion of a ground-ice-rich island in response to arctic summer warming and sea ice reduction. *The Cryosphere*, 9(1), 151–178. <https://doi.org/10.5194/tc-9-151-2015>
- Hayes, S., Lim, M., Whalen, D., Mann, P. J., Fraser, P., Penlington, R., & Martin, J. (2021). Surface and internal data collected from Peninsula point, NWT, Canada between 2016 to 2018 (version 1) [Dataset]. Zenodo. <https://doi.org/10.5281/zenodo.4770736>
- Heginbottom, J. A. (1984). *Continued headwall retreat of a retrogressive thaw flow slide, eastern Melville Island, Northwest Territories*. Geological Survey of Canada, Current Research part B, Paper, (pp. 363–365). <https://doi.org/10.4095/119594>
- Irrgang, A. M., Bendixen, M., Farquharson, L. M., Baranskaya, A. V., Erikson, L. H., Gibbs, A. E., et al. (2022). Drivers, dynamics and impacts of changing Arctic coasts. *Nature Reviews Earth & Environment*, 3(1), 39–54. <https://doi.org/10.1038/s43017-021-00232-1>
- James, M. R., & Robson, S. (2012). Straightforward reconstruction of 3D surfaces and topography with a camera: Accuracy and geoscience application. *Journal of Geophysical Research*, 117(F3). <https://doi.org/10.1029/2011JF002289>
- Johannessen, O. M., Kuzmina, S. I., Bobylev, L. P., & Miles, M. W. (2016). Surface air temperature variability and trends in the Arctic: New amplification assessment and regionalisation. *Tellus A: Dynamic Meteorology and Oceanography*, 68(1), 28234. <https://doi.org/10.3402/tellusa.v68.28234>
- Jones, B. M., Farquharson, L. M., Baughman, C. A., Buzard, R. M., Arp, C. D., Grosse, G., et al. (2018). A decade of remotely sensed observations highlight complex processes linked to coastal permafrost bluff erosion in the Arctic. *Environmental Research Letters*, 13(11), 115001. <https://doi.org/10.1088/1748-9326/aae471>
- Jones, B. M., Hinkel, K. M., Arp, C. D., & Eisner, W. R. (2008). Modern erosion rates and loss of coastal features and sites, Beaufort Sea coastline, Alaska. *Arctic*, 61(4), 361–372. <https://doi.org/10.14430/arctic44>
- Kokelj, S. V., Tunnicliffe, J., Lacelle, D., Lantz, T. C., Chin, K. S., & Fraser, R. (2015). Increased precipitation drives mega slump development and destabilization of ice-rich permafrost terrain, northwestern Canada. *Global and Planetary Change*, 129, 56–68. <https://doi.org/10.1016/j.gloplacha.2015.02.008>
- Lakeman, T. R., & England, J. H. (2012). Paleoglaciological insights from the age and morphology of the Jesse moraine belt, western Canadian Arctic. *Quaternary Science Reviews*, 47, 82–100. <https://doi.org/10.1016/j.quascirev.2012.04.018>
- Lantuit, H., Pollard, W. H., Couture, N., Fritz, M., Schirmermeister, L., Meyer, H., & Hubberten, H. W. (2012). Modern and late Holocene retrogressive thaw slump activity on the Yukon coastal plain and Herschel Island, Yukon Territory, Canada. *Permafrost and Periglacial Processes*, 23(1), 39–51. <https://doi.org/10.1002/ppp.1731>
- Letterly, A. (2018). The recent state of permafrost, 2017–2018. *Global Cryosphere Watch*. Retrieved from: <https://globalcryospherewatch.org/assessments/permafrost/>
- Lewkowicz, A. G. (1987). Headwall retreat of ground-ice slumps, Banks Island, Northwest Territories. *Canadian Journal of Earth Sciences*, 24(6), 1077–1085. <https://doi.org/10.1139/e87-105>
- Lewkowicz, A. G., & Way, R. G. (2019). Extremes of summer climate trigger thousands of thermokarst landslides in a high Arctic environment. *Nature Communications*, 10(1), 1329. <https://doi.org/10.1038/s41467-019-09314-7>
- Lim, M., Whalen, D., Martin, J., Mann, P. J., Hayes, S., Fraser, P., et al. (2020). Massive ice control on permafrost coast erosion and sensitivity. *Geophysical Research Letters*, 47(17). <https://doi.org/10.1029/2020GL087917>
- Mackay, J. R. (1963). *The Mackenzie delta area, N.W.T.* Queen's printer. Retrieved from <https://books.google.co.uk/books?id=MWfIMgAACAAJ>
- Mackay, J. R. (1971). The origin of massive icy beds in permafrost, western Arctic coast, Canada. *Canadian Journal of Earth Sciences*, 8(4), 397–422. <https://doi.org/10.1139/e71-043>
- Mackay, J. R. (1986). Fifty years (1935–1985) of coastal retreat west of Tuktoyaktuk, District of Mackenzie. *Geological Survey of Canada*, 727–735. <https://doi.org/10.4095/120445>
- Mackay, J. R., & Dallimore, S. R. (1992). Massive ice of the Tuktoyaktuk area, western Arctic coast, Canada. *Canadian Journal of Earth Sciences*, 29(6), 1235–1249. <https://doi.org/10.1139/e92-099>
- Markus, T., Stroeve, J. C., & Miller, J. (2009). Recent changes in Arctic sea ice melt onset, freeze up, and melt season length. *Journal of Geophysical Research*, 114(C12), C12024. <https://doi.org/10.1029/2009JC005436>
- Mars, J. C., & Houseknecht, D. W. (2007). Quantitative remote sensing study indicates doubling of coastal erosion rate in past 50 yr along a segment of the Arctic coast of Alaska. *Geology*, 35(7), 583–586. <https://doi.org/10.1130/G23672A.1>
- Moorman, B. J., Michel, F. A., & Wilson, A. T. (1998). The development of tabular massive ground ice at Peninsula Point, NWT, Canada. In A. G. Lewkowicz & M. Allard (Eds.), *Proceedings of the seventh international conference on permafrost*, Collection Nordcanada (Vol. 57, pp. 757–762).
- Murton, J. B., Whiteman, C. A., Waller, R. I., Pollard, W. H., Clark, I. D., & Dallimore, S. R. (2005). Basal ice facies and supraglacial melt-out till of the Laurentide ice sheet, Tuktoyaktuk Coastlands, western Arctic Canada. *Quaternary Science Reviews*, 24(5–6), 681–708. <https://doi.org/10.1016/j.quascirev.2004.06.008>
- Nakamura, Y. (1989). *A method for dynamic characteristics estimation of subsurface using microtremor on the ground surface* (Vol. 30). Railway Technical Research Institute, Quarterly Reports. <https://doi.org/10.1109/IGARSS.2015.7326874>
- Novikova, A., Belova, N., Baranskaya, A., Aleksyutina, D., Maslakov, A., Zelenin, E., et al. (2018). Dynamics of permafrost coasts of Baydaratskaya Bay (Kara Sea) based on multi-temporal remote sensing data. *Remote Sensing*, 10(9), 1481. <https://doi.org/10.3390/rs10091481>
- Obu, J., Lantuit, H., Fritz, M., Pollard, W. H., Sachs, T., & Günther, F. (2016). Relation between planimetric and volumetric measurements of permafrost coast erosion: A case study from Herschel Island, western Canadian Arctic. *Polar Research*, 35(1), 30313. <https://doi.org/10.3402/polar.v35.30313>
- Pix4Dmapper. (2016). Pix4D SA, Switzerland. [Software]. Retrieved from <https://www.pix4d.com/product/pix4dmapper-photogrammetry-software>
- Pizhankova, E. I. (2016). Modern climate change at high latitudes and its influence on the coastal dynamics of the Dmitriy Laptev Strait area. *Earth's Cryosphere*, 20(1), 46–59.

- Pollard, W. H. (1990). The nature and origin of ground ice in the Herschel Island area, Yukon Territory. In *Proceedings, fifth Canadian permafrost conference* (pp. 23–30).
- Ramage, J. L., Irrgang, A. M., Herzsuh, U., Morgenstern, A., Couture, N., & Lantuit, H. (2017). Terrain controls on the occurrence of coastal retrogressive thaw slumps along the Yukon Coast, Canada. *Journal of Geophysical Research: Earth Surface*, *122*(9), 1619–1634. <https://doi.org/10.1002/2017JF004231>
- Ramage, J. L., Irrgang, A. M., Morgenstern, A., & Lantuit, H. (2018). Increasing coastal slump activity impacts the release of sediment and organic carbon into the Arctic Ocean. *Biogeosciences*, *15*(5), 1483–1495. <https://doi.org/10.5194/bg-15-1483-2018>
- Robinson, S. D. (2000). Thaw-slump-derived thermokarst near Hot Weather Creek, Ellesmere Island, Nunavut. In M. Garneau & B. T. Alt (Eds.), *Environmental response to climate change in the Canadian high Arctic* (Vol. 529, pp. 335–345). Geological Survey of Canada.
- Rudy, A. C. A., Lamoureux, S. F., Kokelj, S. V., Smith, I. R., & England, J. H. (2017). Accelerating thermokarst transforms ice-cored terrain triggering a downstream cascade to the ocean. *Geophysical Research Letters*, *44*(21), 11–080. <https://doi.org/10.1002/2017GL074912>
- Scheib, A. J. (2014). *The application of passive seismic to estimate cover thickness in greenfields areas of western Australia—method, data interpretation and recommendations*. Geological Survey of Western Australia, Record, (Vol. 201).
- Segal, R. A., Lantz, T. C., & Kokelj, S. V. (2016). Acceleration of thaw slump activity in glaciated landscapes of the Western Canadian Arctic. *Environmental Research Letters*, *11*(3), 034025. <https://doi.org/10.1088/1748-9326/11/3/034025>
- Serreze, M. C., & Francis, J. A. (2006). The arctic amplification debate. *Climatic Change*, *76*(3–4), 241–264. <https://doi.org/10.1007/s10584-005-9017-y>
- Steele, M., Ermold, W., & Zhang, J. (2008). Arctic Ocean surface warming trends over the past 100 years. *Geophysical Research Letters*, *35*(2), 1–6. <https://doi.org/10.1029/2007GL031651>
- Stroeve, J. C., Markus, T., Boisvert, L., Miller, J., & Barrett, A. (2014). Changes in Arctic melt season and implications for sea ice loss. *Geophysical Research Letters*, *41*(4), 1216–1225. <https://doi.org/10.1002/2013GL058951>
- Swanson, D. K., & Nolan, M. (2018). Growth of retrogressive thaw slumps in the Noatak Valley, Alaska, 2010–2016, measured by airborne photogrammetry. *Remote Sensing*, *10*(7), 983. <https://doi.org/10.3390/rs10070983>
- Tallett-Williams, S., Gosh, B., Wilkinson, S., Fenton, C., Burton, P., Whitworth, M., et al. (2016). Site amplification in the Kathmandu Valley during the 2015 M7.6 Gorkha, Nepal earthquake. *Bulletin of Earthquake Engineering*, *14*(12), 3301–3315. <https://doi.org/10.1007/s10518-016-0003-8>
- Wang, B., Paudel, B., & Li, H. (2009). Retrogression characteristics of landslides in fine-grained permafrost soils, Mackenzie Valley, Canada. *Landslides*, *6*(2), 121–127. <https://doi.org/10.1007/s10346-009-0150-y>
- Wang, B., Paudel, B., & Li, H. (2016). Behaviour of retrogressive thaw slumps in northern Canada—three-year monitoring results from 18 sites. *Landslides*, *13*(1), 1–8. <https://doi.org/10.1007/s10346-014-0549-y>
- Ward Jones, M. K., & Pollard, W. H. (2021). Daily field observations of retrogressive thaw slump dynamics in the Canadian high Arctic. *Arctic*, *74*(3), 339–354. <https://doi.org/10.14430/arctic73377>
- Ward Jones, M. K., Pollard, W. H., & Jones, B. M. (2019). Rapid initialization of retrogressive thaw slumps in the Canadian high Arctic and their response to climate and terrain factors. *Environmental Research Letters*, *14*(5), 055006. <https://doi.org/10.1088/1748-9326/ab12fd>
- Westoby, M. J., Brasington, J., Glasser, N. F., Hambrey, M. J., & Reynolds, J. M. (2012). ‘Structure-from-Motion’ photogrammetry: A low-cost, effective tool for geoscience applications. *Geomorphology*, *179*, 300–314. <https://doi.org/10.1016/j.geomorph.2012.08.021>
- Westoby, M. J., Lim, M., Hogg, M., Pound, M. J., Dunlop, L., & Woodward, J. (2018). Cost-effective erosion monitoring of coastal cliffs. *Coastal Engineering*, *138*, 152–164. <https://doi.org/10.1016/j.coastaleng.2018.04.008>
- Zwieback, S., Boike, J., Marsh, P., & Berg, A. (2020). Debris cover on thaw slumps and its insulative role in a warming climate. *Earth Surface Processes and Landforms*, *45*(11), 2631–2646. <https://doi.org/10.1002/esp.4919>
- Zwieback, S., Kokelj, S. V., Günther, F., Boike, J., Grosse, G., & Hajnsek, I. (2018). Sub-seasonal thaw slump mass wasting is not consistently energy limited at the landscape scale. *The Cryosphere*, *12*(2), 549–564. <https://doi.org/10.3929/ethz-b-000244496>